OPEN ACCESS
IOP Publishing | Royal Swedish Academy of Sciences Physica Scripta
Phys. Scr. 90 (2015) 048002 (15pp) doi:10.1088/0031-8949/90/4/048002

Invited Comment

Experiments in electron microscopy: from metals to nerves

Nigel Unwin

MRC Laboratory of Molecular Biology, Francis Crick Avenue Cambridge CB2 0QH, UK

E-mail: unwin@mrc-lmb.cam.ac.uk

Received 8 October 2014, revised 14 December 2014
Accepted for publication 23 February 2015
Published 17 March 2015

Abstract

Electron microscopy has advanced remarkably as a tool for biological structure research since the development of methods to examine radiation-sensitive unstained specimens and the introduction of cryo-techniques. Structures of biological molecules at near-atomic resolution can now be obtained from images of single particles as well as crystalline arrays. It has also become possible to analyze structures of molecules in their functional context, i.e. in their natural membrane or cellular setting, and in an ionic environment like that in living tissue. Electron microscopy is thus opening ways to answer definitively questions about physiological mechanisms. Here I recall a number of experiments contributing to, and benefiting from the technical advances that have taken place. I begin—in the spirit of this crystallography series—with some biographical background, and then sketch the path to an analysis by time-resolved microscopy of the opening mechanism of an ion channel (nicotinic acetylcholine receptor). This analysis illustrates how electron imaging can be combined with freeze-trapping to illuminate a transient biological event: in our case, chemical-to-electrical transduction at the nerve-muscle synapse.

Keywords: time-resolved electron microscopy, radiation damage, synaptic transmission, structural mechanisms, bacteriorhodopsin, gap junctions, acetylcholine receptor

(Some figures may appear in colour only in the online journal)

Seizing opportunities

I grew up in a happy and supportive household in Christchurch, New Zealand: my father was a paediatrician and my mother a housewife. During the school holidays I would set up projects for myself, and for several years spent much of my spare time building an 8 inch reflecting telescope. Besides a sense of achievement derived from evaluating and improving the optical quality of the mirror as it was being ground out from a thick glass disk, I became fascinated with the properties of the different metals that were required for a well-functioning instrument. Strength and lightness were obvious considerations, but other interesting properties became apparent while attempting to shape various components with metal-working tools.

I think now I was lucky to have had only one close-to-serious accident during this period of unsupervised, at-home experimentation. It occurred near the finishing-off stage, when casting a lead counter-weight to achieve the correct balance of the telescope tube on its equatorial mounting. The melting of lead strips, acquired from local plumbers, was easily done using an old saucepan on the kitchen stove. But in attempting to overcome a problem with the lead sticking to the clay mould, I decided to coat the exposed clay surface with a layer of vaseline. Of course, in hindsight this was not a sensible thing to do. The molten lead, when poured into the grease-coated mould simply exploded in my face!

Fortunately, I was left with only one smallish scar on my left temple. But perhaps this also was an auspicious event: the whole project was a uniquely rewarding experience and its dramatic ending had forged this firmly in my mind.

It was not until I left school, had one clear night proudly resolved the Cassini Division in Saturn's rings, and had completed my first year of an engineering degree at the University of Canterbury, that an opportunity arose to become involved with metals once again. Standard practice would have been to continue at Canterbury, but I realised I could instead apply to the Otago School of Mines, in Dunedin, to continue toward a degree specialising in metallurgy. The latter option made the most sense. It seemed a natural way to extend my schoolboy passion; furthermore, the metallurgy community was small, seeming to provide a better chance to compete successfully and thereby attain the high grade needed for further pursuits.

The logic worked. Soon after I had obtained an engineering degree at the Otago School of Mines I applied to various overseas universities to undertake research for a PhD degree. To my immense surprise, Alan Cottrell, then Head of the Metallurgy Department at Cambridge University simply wrote back offering me a place. As a somewhat gauche New Zealander this seemed a quite unbelievable opportunity. In the English summer of 1965 I sailed from Auckland (a 28 day journey), the normal mode of long-distance travel in those days. As it turned out, by the time I got to Cambridge, Cottrell, who was one of Britain's most distinguished scientists, had already left the Department to become Chief Scientific Advisor to the Ministry of Defence. Instead his colleague, Robin Nicholson (later also Chief Scientific Advisor to the Government) offered me an ideal project to work on: 'the microstructure and fracture toughness of high strength aluminium alloys'.

'Ideal' was the right word: not only did the project encompass study of metals, but also it implicated in a central way another imaging tool—the electron microscope. Transmission electron microscopy of metals was a relatively new discipline in the 1960s, being pioneered by physicists [1], many of whom were working in the Cavendish Laboratory next door. To begin to examine the microstructure of a new alloy, seemed like exploration in the true sense of the word. There was no knowing what you were going to see next. Understandably, I found my graduate research, underpinned by two Siemens electron microscopes named Agatha and Bertha, totally absorbing. In this climate of discovery and with support from some wonderful colleagues, it was a productive two-and-a-half years [2–5].

One goal of my graduate research was to understand the factors affecting the nucleation and growth of small precipitates at the boundaries between neighbouring metal crystals. This was an important topic because cracks leading to catastrophic fractures often propagate along these regions, and the distribution of the precipitates influences the brittleness and susceptibility to stress corrosion of the bulk material. I found that a key parameter affecting precipitation was the relative orientation of the two crystals making the boundary layer. This relationship could be determined precisely from

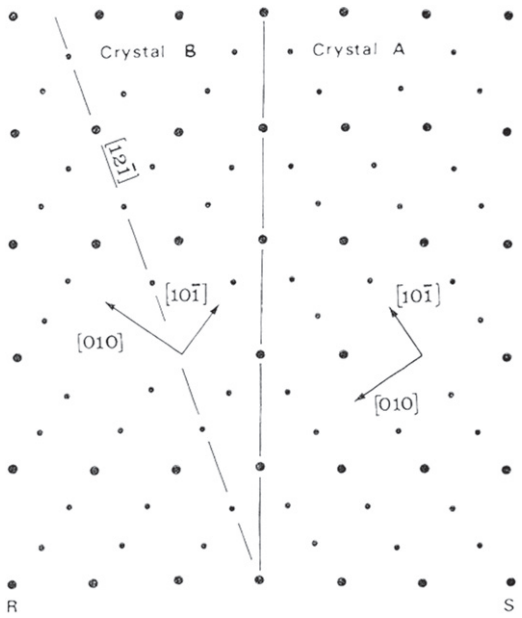

Figure 1. A $\sum = 3$ coincidence site lattice relating two metal crystals, A and B. This lattice (large dots) is shared by both crystals and gives rise to a simple boundary structure [4].

features (Kikuchi lines) in the pair of electron diffraction patterns, and quite frequently it was explicable in terms of a coincidence site lattice [6, 7], in which both crystals share the same superlattice (figure 1). Such a simple result, when it happened, contrasted with the complexity of the analysis required, and was a source of considerable satisfaction. Remarkably, coincidence site lattices were to reappear in a different context some ten years later, when describing the packing of crystalline sheets of ribosomes in the oocytes of hibernating lizards [8].

It seemed as though this introduction to crystallography, involving coincidence site lattices and electron diffraction, had fostered a deeper appreciation of the natural beauty of ordered objects and hence a desire to continue in the same vein. As far as metals were concerned however, it appeared that the scope and opportunities were becoming rather limited. I could investigate a new alloy having a different composition, but fundamental microstructural elements, such as dislocations, stacking faults and Guinier–Preston zones, had by now been described and largely understood. What if I were to switch fields at this stage and instead of metals, use the microscope to look at ordered biological assemblies like muscle filaments and viruses?

The one person I wrote to for advice was my great uncle, Sir Stanley Unwin, founder of the London publishing firm, Allen and Unwin. I did not know him well, but family stories had led me to hold him in great esteem. I emphasized in the letter my concern that I was not fit to make this transition as I had no formal training in biology apart from what I had learned at school. His response was most reassuring: 'I should not have thought that once you had your PhD there would be any question of your having to go back and do two years of undergraduate training in biology. Your knowledge of

electron microscopy, x-rays etc should enable you to go right ahead on biological research'.

Great uncle Stanley was not a scientist. Nevertheless his words clearly had a galvanising effect, because soon afterwards I managed to make an appointment with Hugh Huxley at the nearby MRC Laboratory of Molecular Biology (LMB) to obtain some guidance. Hugh was already well known for his sliding filament model explaining how muscle contracts, and I was inspired to learn that he also had no formal biological training. Later that same week, and to my huge delight, he offered me a position! I could work with the electron microscope with the aim of improving current techniques to obtain better images of biological molecules.

I took the job, but nevertheless the next two years were to be the bleakest of my career. Hugh was one of the pioneers of the negative staining technique, whereby the shape or surface details of a protein are revealed indirectly through the contrast provided by a heavy metal salt. He had recently applied the technique very successfully to discover some remarkable features of the thin and thick filaments isolated from disrupted muscle fibres [9]. He was a superb experimentalist and what could I do to build on what he had already achieved? Furthermore, it was hard to retain confidence in this new environment of cutting-edge biological research (where several of the scientists had Nobel prizes, or were to receive them in the near future). The language of molecular biology seemed totally alien. During my metallurgy days I had sometimes performed amateur dissections on rats and frogs in my college room, but this did not constitute a relevant link. It certainly was not true, as I had supposed, that research at LMB—being in the life sciences—would be easy.

Progress at last

One completely accidental discovery eventually saved me. I was attempting to observe ferritin molecules by dark-field imaging, an approach commonly used to highlight defects in metals, and had placed a thin wire across the objective aperture to block out the direct (unscattered) electron beam. The result was meaningless, but surprisingly, if the diameter of the direct beam was adjusted to be slightly larger than that of the wire, and the specimen was in exact focus, a sharp, high contrast image sometimes appeared fleetingly on the screen. The transient nature of this image indicated electrostatic charging was involved. That is, a voltage was being developed by ejection of secondary electrons at the centre of the wire, but without a proper balance being attained as a result of conduction along the wire or by capture of secondary electrons ejected from other regions. Indeed, in a later series of interference experiments, I was able to manipulate and measure the voltage developed on a thin wire under different illumination conditions and also determine the resulting deflection (hence phase shifts) of the passing 100 KV electrons as a function of distance [10].

These experiments formed the basis for constructing a more precise electrostatic device (figure 2(a)) that would operate like the phase plate of light microscopy, where a uniform phase shift is introduced to enhance the contrast equally over a wide range of object spacings [11]. The electric field created by the charge in the central region needed to be cylindrical, producing a phase shift that increased linearly with distance, but more spherical further out, producing a constant phase shift. Such conditions were best met by having a very thin thread (<0.5 μm in diameter) suspended centrally over a small (30 μm) aperture. The thread of a small spider was ideal for this purpose, and although a bare spider's thread would charge up uncontrollably in the electron beam, a small stable voltage was readily produced after evaporating a thin coat of gold onto its surface. The correct voltage at the middle of the thread could then be fine-tuned by minor adjustments of the illumination, leading to a uniform $\sim\pi/2$ phase shift of the scattered electrons out to a resolution of about 5 Å (as demonstrated by optical diffraction of an image of a carbon film; figure 2(b)).

Interestingly, the phase shift introduced by this device is in the same sense as that due to spherical aberration, but opposite to that generated in normal (bright field) imaging by under-focusing. Whereas *dark* phase contrast produced by under-focusing adds to the dark in-focus appearance of the stain, the *bright* phase contrast produced by the phase plate tends to cancel out the dark in-focus appearance of the stain. In imaging negatively stained specimens, therefore, the phase plate diminishes the contribution of the stain to the contrast and enhances preferentially the encased protein. These differences between the two kinds of image are apparent in figure 2(c).

Low dose microscopy

Though the phase plate was difficult to make and so did not become a lasting practical device, it provided some unique insight into the nature of negative staining and highlighted the need to minimize radiation damage. A key conclusion of an analysis of TMV protein (see figure 2(c)) was that the phase plate revealed the narrow helical grooves between subunits more strongly than did the normal (bright field) image [12]. A possible explanation for this, in view of the two different contrast mechanisms, was that the stain, while initially fitting accurately into the grooves, had altered its distribution through radiation damage; whereas the radiation product of the protein (imaged preferentially with the phase plate) maintained better the original morphology.

A study comparing normal images of TMV protein with low dose images (i.e. recorded with no significant pre-irradiation) confirmed that electrons cause the stain to migrate [13]. I observed that stain contracts under the electron beam and rearranges in an orderly way, consistent with its migration over a regular substrate. Furthermore, in three-dimensional maps of the TMV protein obtained by helical reconstruction, the low dose image gave a closer representation of the true structure (indicated by x-ray diffraction [14]) than did the normal image.

While these experiments drew attention to the loss of useful information that accompanies radiation damage, they

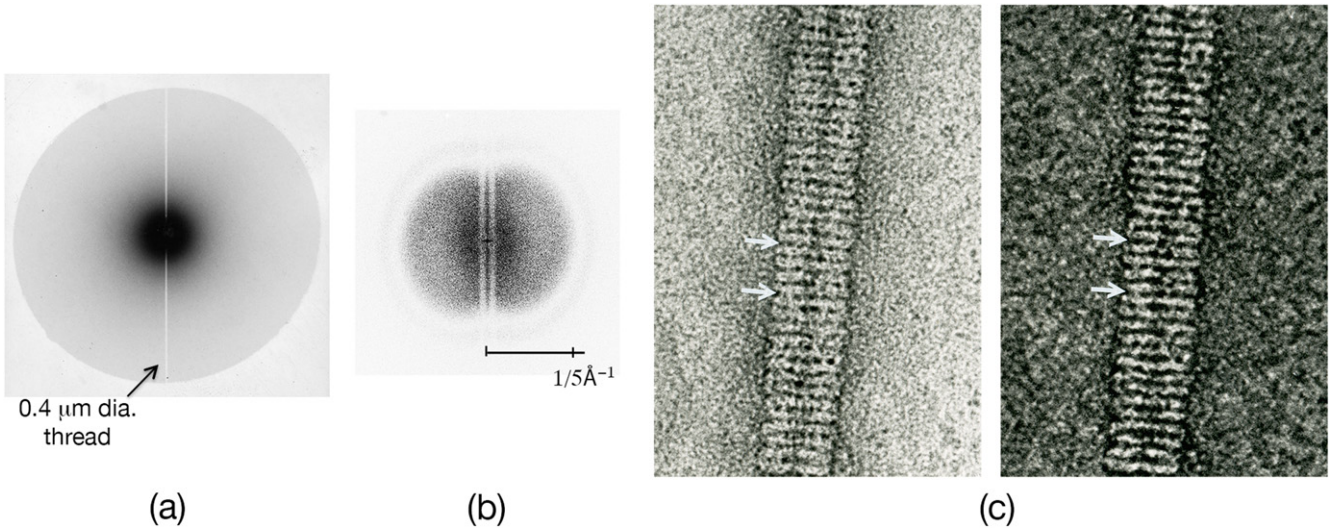

Figure 2. Electrostatic phase plate. (a) Showing the direct beam being intercepted by the thin spider's thread in the diffraction plane of the objective lens; the edge of the 30 μm diameter supporting aperture is also visible. (b) Thon ring pattern from a phase plate image of a carbon film, demonstrating uniform contrast transfer extending to a resolution of ~5 Å. (c) Defocused bright field (left) and phase plate (right) images of the same stacked-disk aggregate of TMV protein. Equivalent regions in the two images, for example between the pair of arrows, show differences in fine detail reflecting different properties of the two kinds of image. Reproduced from [10] and [11].

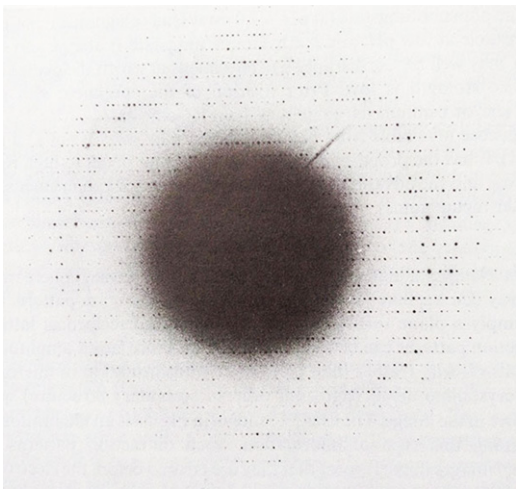

Figure 3. Electron diffraction pattern from a thin catalase platelet embedded in glucose, demonstrating preservation of crystalline order to a resolution of ~3.5 Å. Unit cell dimensions: $a = 69$ Å, $b = 173.5$ Å. Recorded at room temperature.

also stressed the need to investigate the protein without the complications caused by stain, and in a state where its native structure remains intact. One conceivable approach, avoiding dehydration in the microscope vacuum, would be to have the protein embedded in ice and viewed at a temperature low enough to avoid sublimation. Electron diffraction patterns from frozen catalase crystals [15], which could be recorded straightforwardly at very low doses, had demonstrated the potential of this approach. However the cold stages available at this time had not been developed for high resolution imaging, and the rapid-freezing method of specimen preparation [16] was to come later.

As a more practical route to *in vacuo* preservation, would it be possible simply to substitute the aqueous medium with a non-volatile liquid that has similar chemical and physical properties? Indeed I found that a number of small hydrophilic molecules, most especially glucose, fulfilled the requirements, allowing good electron diffraction patterns to be recorded from catalase crystals at room temperature (figure 3). Equally important, high-angle x-ray patterns from these crystals dried in glucose were almost identical to those from crystals kept in solution [17], indicating that the protein retained its native conformation. Now that proper preservation had been achieved, the next step was to record low dose images of the ordered protein arrays and extract the structural information they contained.

Viewing protein directly

The imaging of unstained specimens and ensuing structural analyses were realised in a very fruitful collaboration with my colleague, Richard Henderson. Richard had been using x-ray diffraction to investigate the structure of crystalline membrane patches (purple membranes) isolated from a bacterium that inhabits salt lakes. The embedded protein, bacteriorhodopsin, is of wide interest because it harnesses light photons to drive hydrogen ions across the membrane. Our electron diffraction patterns from single patches showed spots arranged on a hexagonal lattice and extending to high resolution. As with catalase, this was a clear indication that the corresponding images, recorded with a low enough dose, should be able to reveal the structure.

Significant fading of the diffraction patterns occurred while they were being recorded, indicating that very low doses (~1 electron/Å^2) would be needed to keep the molecules fully intact. Accordingly, the image magnification had to be unusually low (~40 000x): otherwise fog from the photographic film would dominate. Stray magnetic fields

Figure 4. Off-axis viewing screen for recording images in low dose microscopy. The area of interest is located (with an extremely low dose) on the optic axis at low magnification, and focusing is performed at the recording magnification with a narrow beam centred on the off-axis screen (arrow). The illumination is then shut off, using a simple mechanical shutter (involving translation of the condenser aperture), but re-established after the beam has been expanded and repositioned to follow an on-axis path. The area of interest thereby receives no significant pre-irradiation before the image is recorded. The equivalent operations are accomplished electronically, without the need for an additional screen, in modern electron microscopes.

were a problem under these conditions, and we found it necessary to insert mu-metal shielding in the projection chamber of the Philips EM301 microscope to prevent significant blurring of the image. Also important were an off-axis viewing screen (figure 4) and a simple mechanical shutter below the condenser lens to minimize beam-induced movement.

The resulting micrographs seemed almost magical: regular features in them were not visible to the naked eye because of the statistical noise due to low numbers of electrons and the low contrast; yet when one shone a laser beam through the photographic plate to make an optical diffraction pattern, spots appeared arranged as they were in the electron diffraction patterns (figure 5(a)). Evidently this was an excellent example of the power of diffraction in separating out a regular signal (lattice of spots) from random noise (intensities between the spots). Of course, in the images the regular information was spread out, rather than concentrated into sharp spots, making it much harder to detect.

In principle, it would be possible to derive a detailed projected structure of an individual molecule (or unit cell) by averaging the information from the many identical copies composing the crystalline array. The averaging would reinforce the genuine features common to each molecule, whereas the random statistical fluctuations would be smeared out. But it was even simpler and more direct to make use of Fourier transforms to perform the equivalent operation, after densitometering the micrographs (using an exceptionally small step size) to convert them into numerical density arrays. This computational approach had already been developed in our Laboratory by David DeRosier and Aaron Klug to reconstruct the shapes of virus particles embedded in negative stain [18]. The phases and amplitudes at the Fourier peaks (corresponding to the diffraction spots) gave us respectively the relative positions and strengths of the sine wave components from which the structure is built. In addition, the Fourier transform made it straightforward to correct for modulations of the contrast transfer function, produced by under-focusing, and to substitute the Fourier amplitudes with more accurate values from electron diffraction. A projection map could then be calculated from the full set of corrected phases and amplitudes by Fourier synthesis. In the case of purple membrane, the resolution attained was 7 Å, enough to show densities characteristic of α-helices clustered around the three-fold axes ([19]; figure 5(b)). It was clear immediately that we were beginning to see the internal structure of a protein.

This was an exciting step, which opened the possibility of determining, from a range of views, what the membrane looks like in three dimensions. We therefore recorded many images and electron diffraction patterns of membrane patches tilted at different angles to the electron beam. These provided new phase and amplitude terms, which we combined in reciprocal space to make plots of the continuous variations along the lattice lines running perpendicular to the membrane plane. The continuous variations in phase and amplitude, after sampling at regular intervals, were then used to calculate a three-dimensional map ([20]; figure 5(c)). Now, in the locations expected from the projected structure, were long, slightly tilted rods of density crossing the membrane from one side to the other. The rods clustered around the three-fold axes in bundles of seven. Unmistakably, these bundles corresponded to a set of seven α-helical segments comprising the structure of bacteriorhodopsin.

Ventures into other systems

The study of purple membrane gave rise to fresh optimism: electron microscopes had yielded resolutions of better than 3 Å in images of metals and minerals, and there seemed no fundamental reason why the same could not be achieved with biological molecules. I was keen therefore to develop a project that would help to advance this technology, while at the same time probing an important biological question.

One potential project was suggested by a picture in Nature News and Views article showing an array of tetrameric ribosomes. The ribosomes were from the oocytes of the S Italian lizard, *Lacerta sicula*, where they form extensive crystalline layers on membranes during winter hibernation (figure 6(a)). Could I image the arrays, after isolating them from the oocytes, and analyze them by our electron crystallographic methods to determine the structure of the ribosome?

I took a train to Naples to visit Carlo Taddei, who had been studying the formation of 'ribosomal bodies' in the oocytes [21], to seek his advice and to collect some lizards. With his help (and apparently, that of the local children) I was

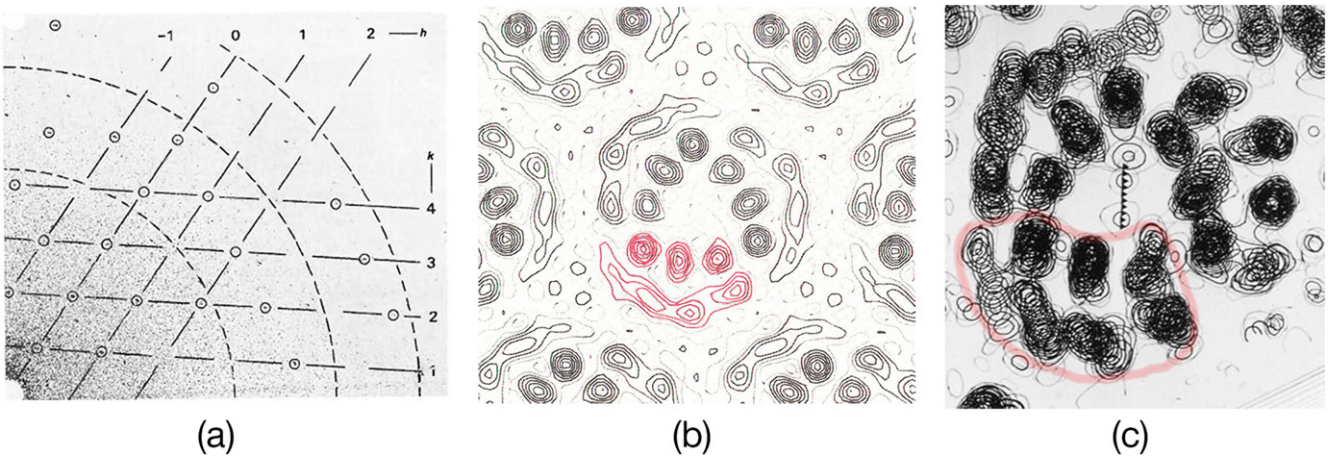

Figure 5. Purple membrane and bacteriorhodopsin. (a) Optical diffraction pattern (quadrant) from a low dose image of purple membrane showing sharp diffraction peaks (hexagonal lattice) superimposed on a background of random noise. The circular arcs indicate the positions of the zeros in the contrast transfer function, determined from a second image recorded with a higher dose. Reproduced from [19]. (b) Contour map of the projected structure of purple membrane at 7 Å resolution, showing bacteriorhodopsin molecules arranged on a $p3$ lattice, unit cell dimension: $a = 62$ Å. One molecule is coloured pink. (c) View of part of the three-dimensional map showing rod-shaped α-helical densities spanning the lipid membrane; a single bacteriorhodopsin molecule, comprised of seven α-helices, is outlined in pink.

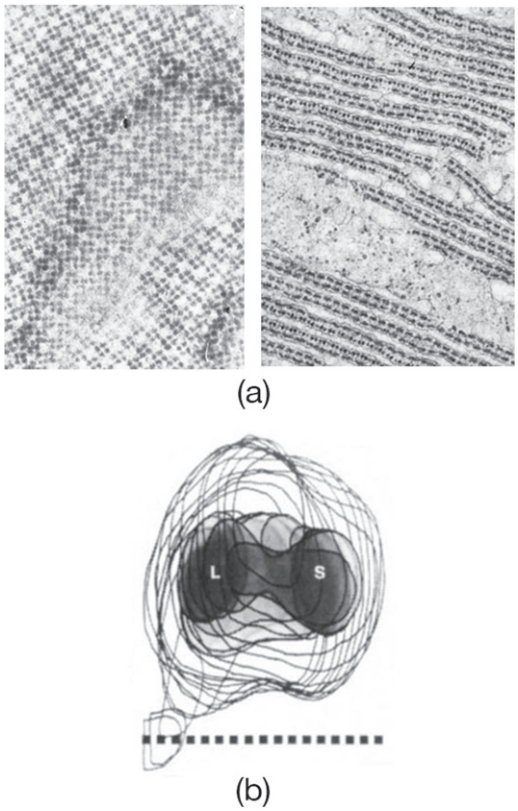

Figure 6. Membrane-bound ribosomes. (a) Face-on (left) and edge-on (right) views of crystalline ribosome layers and membranes in the oocyte of *Lacerta sicula* during winter. The ribosomes in each layer arrange as tetramers on a $p4$ lattice ($a = 595$ Å). The layers associate in pairs between membranes of the endoplasmic reticulum, and attach to them via a salt-sensitive linkage. Plastic embedded thin sections. (b) Single ribosome from a three-dimensional map showing locations of large (L) and small (S) subunits relative to the endoplasmic reticulum membrane (dotted line; [22]).

able to obtain dozens of lizards. I soon learned how to isolate the crystalline layers, grow them at will by cooling the lizards and to characterise them by negative staining. A fascinating finding was that the oppositely-facing layers between adjacent membranes were related to each other by specific rotations, where certain of the tetramers in each layer exactly superposed [8]. The shared 'superlattices' made by the superposing tetramers were generated by precisely the same rules as were the coincidence site lattices used to relate adjacent metallic crystals to one another.

A three-dimensional map obtained from the isolated layers, in stain, showed both ribosomal subunits to be adjacent to the membrane surface, attached to it by a part protruding from the large subunit ([22]; figure 6(b)). This configuration was of particular interest because the attachment was via the same salt-sensitive linkage as is used by membrane-bound ribosomes in secretory cells [23, 24]. Ron Milligan found later that the configuration was such as to place the end of the exit channel for nascent protein close to the membrane attachment site, so that the emerging chain would be optimally located to interact with components of the translocation apparatus [25]. In another study, Werner Kühlbrandt analyzed the distribution of RNA and protein within the lizard ribosomes [26], but short-range disorder limited the information obtainable and, for a number of reasons, it became difficult to progress much further. Clearly this project was overly ambitious: it was to take more than thirty years of effort, and several major technological advances, before the goal of imaging ribosomes at near-atomic resolution was finally achieved [27].

The nuclear pore complex is an organelle, ubiquitous to eukaryotic cells, which serves as a pathway though the nuclear envelope for nuclear and cytoplasmic molecules. I viewed it as another candidate for analysis by the methods we

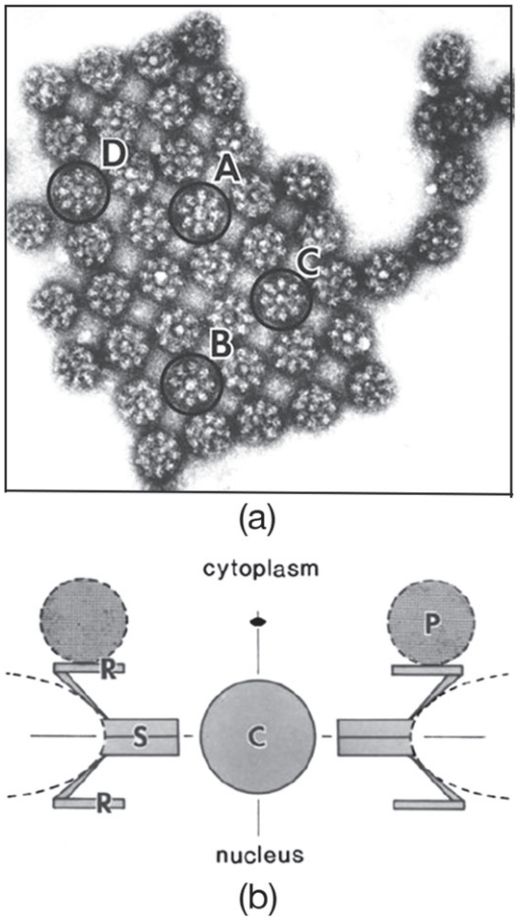

Figure 7. Nuclear pore complexes from *Xenopus* oocytes. (a) Square array of ~1200 Å diameter pore complexes released from the nuclear envelope, in uranyl acetate stain. (b) Architecture determined from a three-dimensional map and selective release experiments [28]. There are several discrete components arranged with octagonal symmetry. Apparent two-fold axes perpendicular to the octad axis suggest that the framework is built from two equal but oppositely facing halves. The half facing the cytoplasm is in some instances decorated by large particles similar in appearance and size to ribosomes.

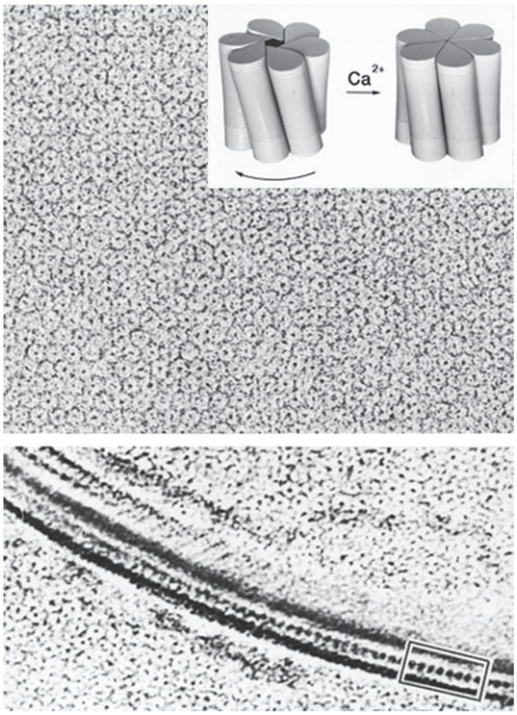

Figure 8. Gap junction plaque isolated from rat liver showing individual channels (connexons) viewed from (upper) a direction perpendicular to the membrane plane and (lower) a direction more nearly parallel to this plane. The channels in the *en face* view appear as annular units arranged on a hexagonal lattice (unit cell dimension: $a = 85$ Å); whereas from the side view, they are seen as bridges (most clear in the boxed area) connecting the two apposed plasma membranes. The inset depicts the transition from the 'open' to the 'closed' configuration, suggested by the three-dimensional maps. Uranyl acetate stain. Reproduced from [30].

had developed, given its symmetrical nature, and the fact that it sometimes forms ordered arrays (figure 7(a)). Nuclear pores could be isolated readily from the nuclear envelopes of *Xenopus* oocytes, where it is present in high concentrations, and we analyzed its architecture by a three-dimensional image analysis combined with selective release experiments ([28]; figure 7(b)). But again only a limited amount of structural information could be obtained, because of disorder and heterogeneity from one pore complex to the next.

Gap junctions are specialised regions of contact between apposed plasma membranes of communicating cells that regulate the flow of ions and small molecules between the two interiors. I was fortunate to have a colleague, Guido Zampighi, who had developed a procedure to isolate these organelles from rat liver in the form of double-layer plaques (figure 8). The plaques contained regular arrays of membrane channels [29], and so seemed promising specimens to investigate further. From images of two kinds of plaque, in negative stain, we obtained two three-dimensional maps [30]. They showed the constituent hexameric channel protein (called a connexon) in either kind of plaque to have different conformations. A comparison of the two alternative conformations suggested a simple way by which the connexon channel might open and close, involving small tilting and sliding motions of adjacent subunits along their lines of contact (figure 8; inset). This iris-like mechanism is attractive from an energetic point of view, since it preserves the hydrophobic partitioning between parts inside and outside the lipid bilayer. But is it a physiological mechanism that would be sensitive to calcium ion concentration or pH?

At this point, it became important to image the gap junction plaques in a controlled ionic environment, as could be done by freezing them in a thin aqueous layer sandwiched between two carbon films [31], and examining them at low temperature. A cold stage was constructed for this purpose [32], and we analyzed plaques in the presence and absence of calcium ions, after first establishing optimal conditions using low-angle x-ray diffraction [33]. The two new three-dimensional maps of the ice-embedded plaques now showed the connexons in their entirety, including the portions traversing the lipid bilayer [34]. Calcium had induced essentially the

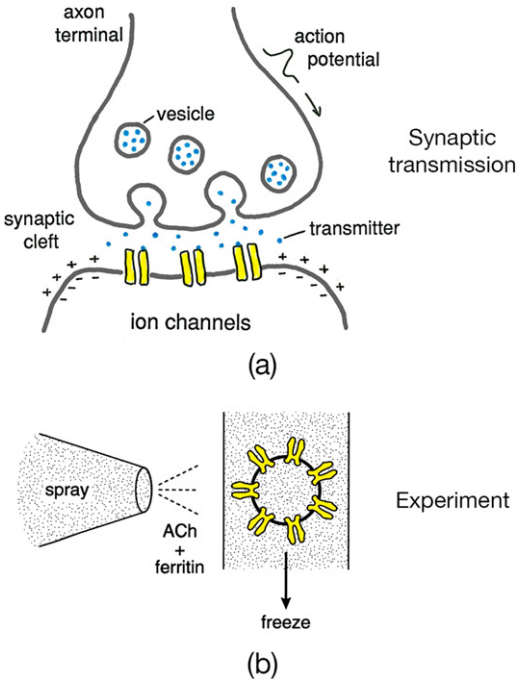

Figure 9. Fast synaptic transmission. (a) The electrical impulse, or action potential, when it reaches the nerve terminal causes vesicles containing a chemical transmitter to release their contents into the synaptic cleft. The transmitter molecules diffuse across the cleft and bind to ligand-gated ion channels in the plasma membrane of the target cell. The binding triggers the channels to open, allowing ions to flow through down their electrochemical gradients, thereby altering the voltage across the target cell membrane. The transient conversion by the channel of a chemical input into an electrical output is a process of chemical-to-electrical transduction. (b) A possible way to recapitulate chemical-to-electrical transduction *in vitro*. The chemical transmitter (in our case acetylcholine) is sprayed onto isolated membrane vesicles containing ion channels (acetylcholine receptors), converting them to an open state, and the reaction is trapped by rapid freezing. Ferritin marker particles are included in the spray solution so that vesicles that have actually been 'hit' by the transmitter can be identified in the images.

same subunit rearrangement as was inferred from the analysis using negative stain. Therefore an iris-like mechanism may indeed play a physiological role, although recent higher resolution studies of the recombinant connexin protein [35, 36] suggest that the actual structural transition may be more complex.

Nicotinic acetylcholine receptor

While these projects just described illuminated to some extent the systems under study, it was not until I had left LMB and joined the faculty at Stanford University (1980–87) that I felt I had found my niche. I taught histology there, and in preparing lectures on wide-ranging topics, the one biological mechanism that, to my mind, stood out above all others in terms of its importance and the need for structural explanation was the mechanism of communication at the chemical synapse (figure 9(a)). How can an electrical pulse be transmitted from a nerve cell to its partner in only a millisecond, given that several quite disparate steps are involved? In particular, how are ion channels in the postsynaptic membrane able to respond so quickly (within microseconds) and robustly to the release by the nerve cell of a chemical transmitter? Finally, can the transient conformational change to open a channel be analyzed directly—by spraying transmitter onto the postsynaptic membranes, and imaging them after trapping the reaction by rapid freezing (figure 9(b))?

An opportunity to look into these questions came about at Stanford while working with Alain Brisson, who at the time was studying protein arrays in bladder membranes. In his graduate research, Alain had discovered that postsynaptic membranes isolated from the electric organ of the *Torpedo* ray (a muscle-derived tissue) sometimes grow into tubular vesicles having acetylcholine receptors arranged regularly on their surface (figure 10(a)). The acetylcholine receptor, better known for its role at the synapse between nerve and muscle cells, is the most thoroughly characterized transmitter-gated ion channel and is remarkable for its high efficacy and speed. In view of its physiological significance and the fact that the *Torpedo* electric organ is a rich and readily available source of the protein, it seemed that this could be the ideal receptor for exploring the structural basis of fast synaptic transmission.

Our investigation of acetylcholine receptor tubes began when we noticed they are strikingly similar in visual appearance to tubes assembled from polyoma virus capsomeres. The capsomeres, originally thought to be hexamers, had recently been shown in low-dose stain images to be pentamers [37]. Given that the number of receptor subunits was controversial, but most likely five or six, would we also see pentamers if we took care to minimize electron dose? Indeed, Fourier analysis of our low dose images showed the receptors to be just like the polyoma capsomeres ([38]; figure 10(b)). In both kinds of tube the protein assemblies form paired pentamers, which pack side-by-side on a $p2$ surface lattice. Moreover, we showed that the pairing observed in the acetylcholine-receptor tubes was due to a disulphide bridge between neighbouring receptors made by the δ subunits [38, 39].

The micrograph of tubular vesicles shown in figure 10(a), was recorded at near liquid-nitrogen temperature from a grid that had been plunge-frozen in liquid ethane. The freezing was so rapid that the specimen became embedded in amorphous, rather than crystalline ice. This specimen preparation method, developed by Jacques Dubochet and his colleagues [16], allows the protein to be well contrasted against the surrounding water and lipids, and is a major advance over the earlier method [31, 34], where ice crystals form. Applied to wide, flattened tubes (as in figure 10(a)), it enabled us to obtain a low resolution three-dimensional map ($P2$ space group), displaying the receptor as a ring of five ~160 Å long rod-shaped subunits ([40]; figure 10(c)). The structure had pseudo-fivefold symmetry, consistent with the by-then-known stoichiometry (α_2, β, γ, δ) and homology between the four polypeptide chains.

Although helpful in initial studies, the wide tubes were unevenly flattened against the carbon support, and would not be appropriate anyway for functional experiments where all

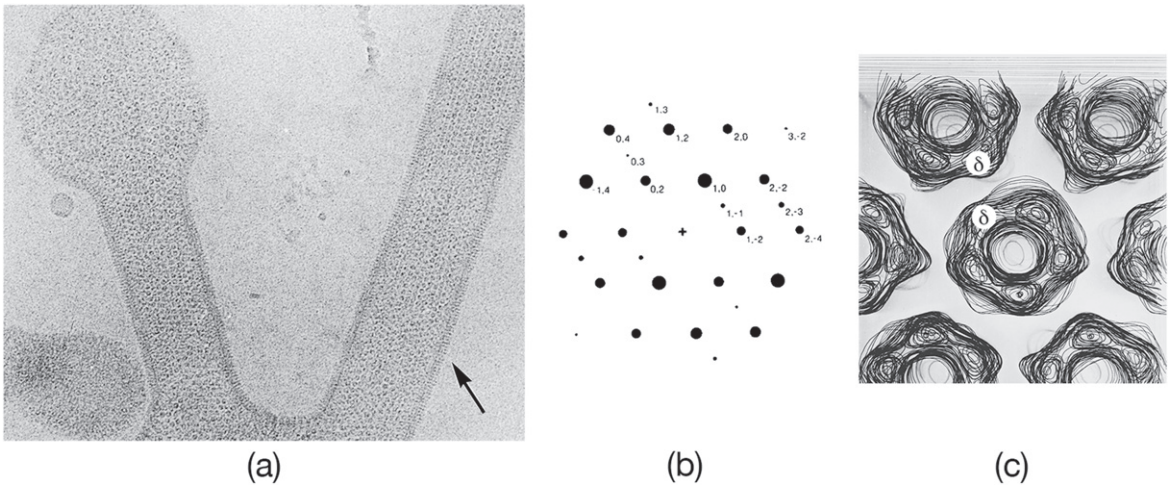

Figure 10. Tubular crystals of acetylcholine receptors. (a) Postsynaptic membrane vesicles forming tubes, embedded in a thin film of frozen solution and flattened on the microscope grid. The complex patterns on the tubes arise from superposition of *en face* views of the receptors located on the top and bottom sides. The striated zones at the tube borders (arrow) are a result of the receptors being viewed more nearly edge-on. The crystalline packing of receptors on the tube surfaces is similar to that found at the synapse *in situ*. (b) Fourier transform from an image of a flattened tube, showing diffraction peaks from the array of receptors on one side. The amplitudes of the peaks are proportional to the shown diameters. The stronger h, k peaks all lie on an approximately hexagonal lattice. The weak peaks, for which k is odd, are associated with a doubling of the b dimension of the surface lattice, due to the pairing of the pentameric receptors. The unit cell dimensions of the $p2$ surface lattice, estimated from the transform are: $a = 90$ Å, $b = 162$ Å, $\gamma = 118°$. (c) Three-dimensional map at 25 Å resolution of receptor molecules in the surface lattice as they would appear viewed from the synaptic cleft. The paired receptors pack side-to-side, forming a ribbon of receptor dimers (see also figure 11) aligning in the horizontal direction. The δ subunits of neighbouring receptors are labeled to indicate the location of the δ–δ disulphide bridge responsible for the observed pairing. Successive sheets are of sections parallel to the membrane plane separated by spaces corresponding to 5 Å; data from ice-embedded, flattened tubes. Reproduced from [38] and [40].

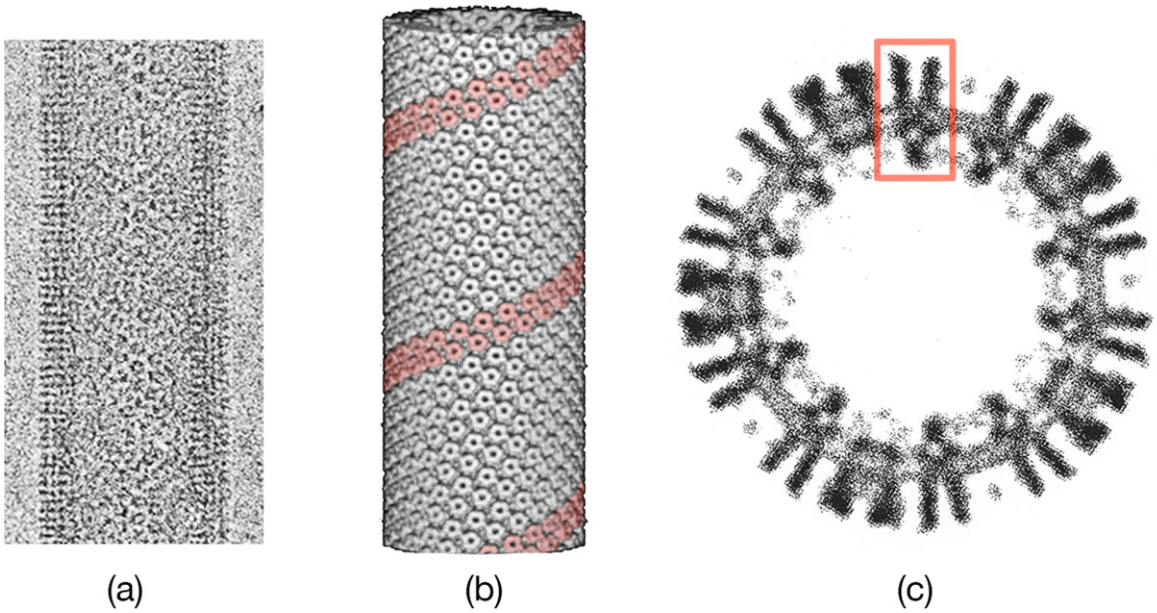

Figure 11. Structure analysis by helical image reconstruction. (a) Electron micrograph of a narrow (~800 Å diameter) tube in amorphous ice, spanning a hole in the carbon support film. (b) Surface representation reconstructed from images of tubes belonging to the (−16, 6) helical family (i.e. having a surface lattice built from a 16-start left-handed helix and a 6-start right-handed helix). The pink shading highlights the basic helix formed by a ribbon of receptor dimers. (c) Cross-section from a reconstruction of a (−15, 5) tube normal to the tube axis, showing the extracellular (outside) and intracellular (inside) portions of the receptors projecting from the phospholipid headgroup regions of the membrane (pair of concentric rings of density, 30 Å apart). A single receptor, cut centrally, is identified by the pink box. Reproduced from [50].

receptors should be equally accessible to acetylcholine. Fortunately these problems could be avoided by directing attention to narrower tubes (<850 Å in diameter) suspended over holes, which after plunge-freezing remain circular in cross-section and face solvent from all sides (figure 11(a)). The surface lattices now formed families of helices, making the tubes amenable to the Fourier method of helical image reconstruction. This method, originally developed by David

DeRosier and Aaron Klug and applied to filamentous stained objects, was extended significantly by Chikashi Toyoshima to enable rigorous analyzes of ice-embedded tubes. Thus it soon became possible to attain a resolution of ~17 Å [41, 42], sufficient to reveal more precisely the overall shape of the receptor (figure 11(b)). The central ion path was now seen as a narrow pore spanning both leaflets of the lipid bilayer and framed on either side by large extracellular and intracellular vestibules (figure 11(c)).

It was to take more than a decade of effort with the narrow tubes to extend the resolution to 4 Å, making it possible to build an atomic model of the receptor. Two things were restricting the information obtainable. First was the presence of distortions, such as variable twisting and slight bending of the tubes in and out of the plane of the microscope grid. These weaken diffraction at higher resolution and needed to be corrected to recover the full signal. Second was the limited performance of commercially available cold stages. My student, Rameen Beroukhim developed a method for correcting for the distortions by dividing the tubes into short segments and aligning them individually to make a more perfect helix [43]. A long and rewarding collaboration with Yoshi Fujiyoshi (who had constructed an exceptionally stable liquid helium-cooled stage [44]) and his postdoctoral assistant Atsuo Miyazawa, enabled us to acquire the large number of high quality images that were needed [45].

The atomic model derived from the 4 Å density map finally revealed the intricate folding of the α_γ, β, δ, α_δ and γ polypeptide chains ([46, 47]; figure 12). Each subunit is a long rod divided into three distinct parts (figure 12(a)): an N-terminal extracellular portion organized around a β-sandwich core, a membrane-spanning portion comprised of four α-helices and an intracellular portion containing one α-helix. The individual subunits arrange side-by-side, forming a pseudo-fivefold symmetric assembly (figure 12(b)) having three functionally distinct domains (figure 12(c)). The extracellular domain harbours two acetylcholine-binding sites, which are in the α subunits at the interfaces with neighbouring γ and δ subunits (between loop C and the co-ordinating tryptophan residue, W149). The membrane domain contains the gate of the channel. The intracellular domain shapes five side-windows for ions passing into (or from) the interior of the cell.

Perhaps the most surprising aspect of the structure is the design of the membrane pore. The pore is lined by five bent α-helices (M2; figure 12(a)), one from each subunit. They come together symmetrically near the middle of the membrane, and conserved hydrophobic side-chains projecting inward in this region create a constricting girdle that is about 8 Å long and 6 Å across. The diameter of this constriction may seem large, given that the structure is of the receptor in the resting state, where the pore is closed (a bare sodium ion, for example, has a diameter of 1.9 Å). However the hydrophobic girdle contains no polar groups that would electrostatically stabilize the ion. Yet in retaining its tightly bound hydration shell, the ion is, in effect, too big to pass through. Therefore gate of this channel should be considered as an energy barrier, rather than a physical barrier, to ion permeation across the membrane. The wide diameter and hydrophobic nature of the constriction ensure that only minor changes in this region will be sufficient to make a fully conducting pore [48].

Time-resolved microscopy

In living tissue, activated acetylcholine receptors revert quickly to the closed-channel form, due to the action of the enzyme, acetylcholinesterase, which depletes acetylcholine from the synaptic cleft. In the continued presence of acetylcholine, on the other hand, the receptors soon (within ~20 ms) become desensitised. In a spray-freezing experiment to capture the open channel (as sketched in figure 9(b)), it is therefore essential to trap the reaction after only a few milliseconds. Provided this is done, and the local concentration of acetylcholine is above saturating amounts (~50 μM), the probability of the channels being open is extremely high (>90%; [49]).

The narrow acetylcholine-receptor tubes made excellent specimens for this experiment. First, they are outside-out vesicles, exposing directly the extracellular binding sites to the sprayed ligand. Second, they present the receptor fully intact, in its natural membrane setting and with molecular packing similar to that found *in situ* [50]. Third, their helical surface lattice allows three-dimensional reconstructions to be made from single images, so that the effect of the transient reaction with acetylcholine in each image can be quantitatively assessed.

The native composition of the tubular membranes is especially important because the functioning receptor is exquisitely sensitive to the lipid environment, and converts to a non-activatable uncoupled conformation if anionic lipids and/or cholesterol are absent [51, 52].

Figure 13 shows the apparatus designed to achieve the required time resolution, while enabling the specimens—the narrow tubes—to be imaged later in the electron microscope [53]. The grid is blotted in the normal way and plunged into liquid ethane. As it falls it is intercepted by the acetylcholine-containing spray, emanating from a nozzle located just above the ethane surface. The resultant reaction time, up to 10 ms, is short enough to prevent desensitization, yet long enough to allow the droplets to coalesce completely with the aqueous film on the grid. Originally ferritin marker particles, included in the spray solution, were used to identify the activated tubes in the images. However in a later refinement of this technique, tubes in the 'diffusion zone' [53], beyond the ferritin-delineated edges of the spreading droplets, could also be identified, based on reference matching [54]. In this zone, the estimated acetylcholine concentrations and reaction time-scales were 50 μM–1 mM and 0–2 ms respectively, recapitulating almost perfectly the conditions for activation at the nerve-muscle synapse [55].

Chemical-to-electrical transduction

By applying this time-resolved method to a large number of the narrow tubes, we obtained a 6 Å structure of the acetylcholine receptor in the open-channel form [54]. Comparison

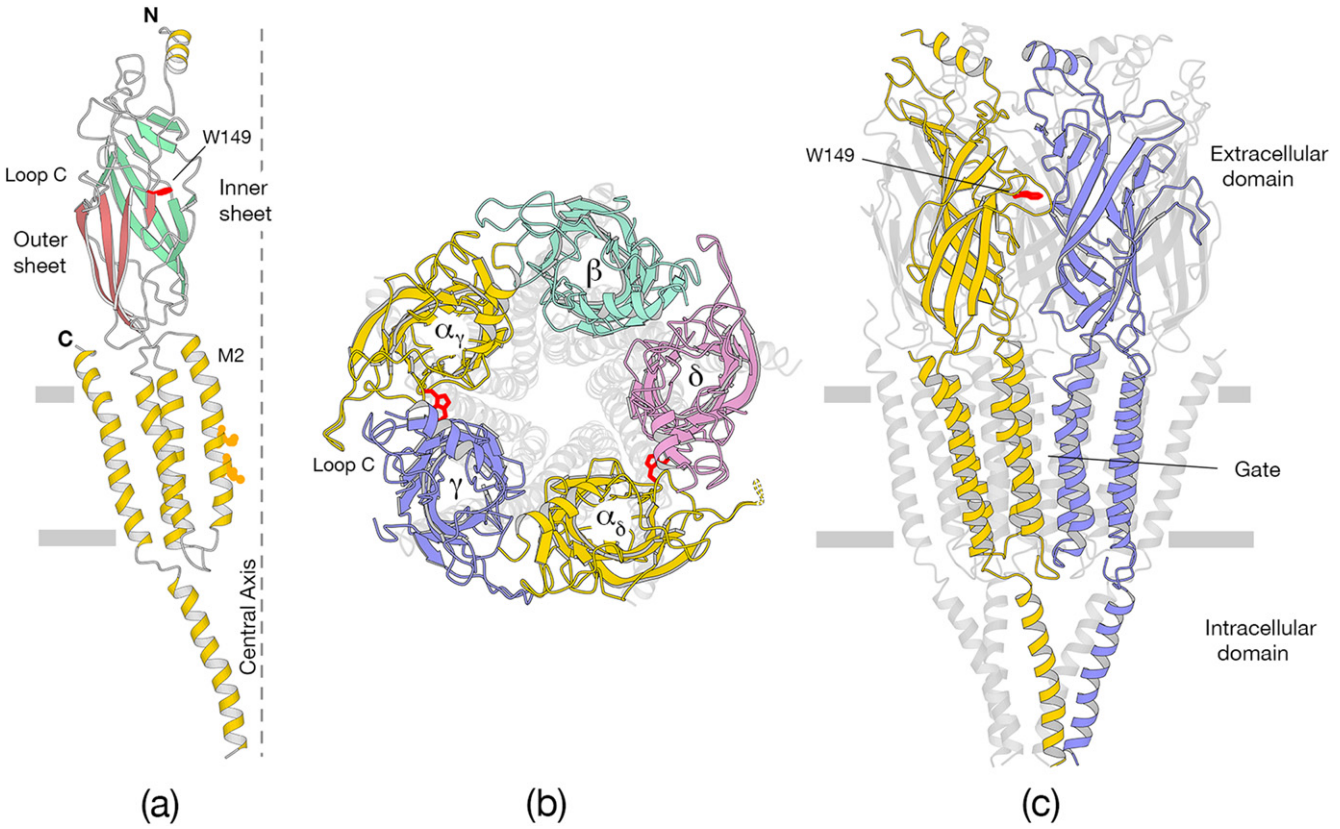

Figure 12. Architecture and fold of the acetylcholine receptor determined from electron micrographs recorded at 4 K. (a) The α_γ subunit viewed from the side, with the central axis of the receptor on the right. The outer and inner sheets composing the β-sandwich core are in pink and green, respectively. Acetylcholine binds in the region between loop C and W149. Conserved valine and leucine side-chains projecting from the pore-lining α-helix, M2, are involved in forming the gate. (b) Whole assembly as viewed from the synaptic cleft, with individual subunits identified around the ring. (c) Whole assembly viewed from the side, with the α_γ and γ subunits in the foreground. The gate of the channel, in the middle of the membrane, is more than 50 Å from the acetylcholine binding sites. The position of the membrane is indicated in (a) and (c) by the horizontal bars.

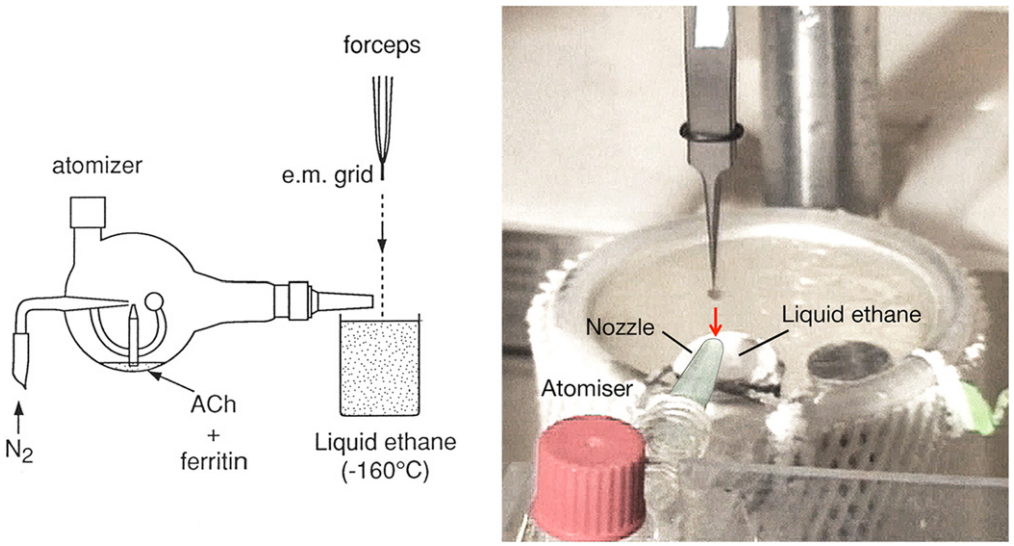

Figure 13. Spray-freeze-trapping: diagram of the apparatus and picture showing the grid being plunged by free-fall into liquid-nitrogen-cooled ethane. The grid contains the specimen in a thin aqueous film and, just before hitting the ethane surface, it is intercepted by a fine spray of acetylcholine droplets, which spread over and mix with the contents of the film. The atomizer produces a pulse of concentrated ~1 μm diameter droplets. Its nozzle is located only a short distance above the ethane surface to keep the maximum reaction time brief (~10 ms). Ferritin marker particles are included in the spray solution so that tubes that have actually been exposed to acetylcholine are readily identifiable in the images.

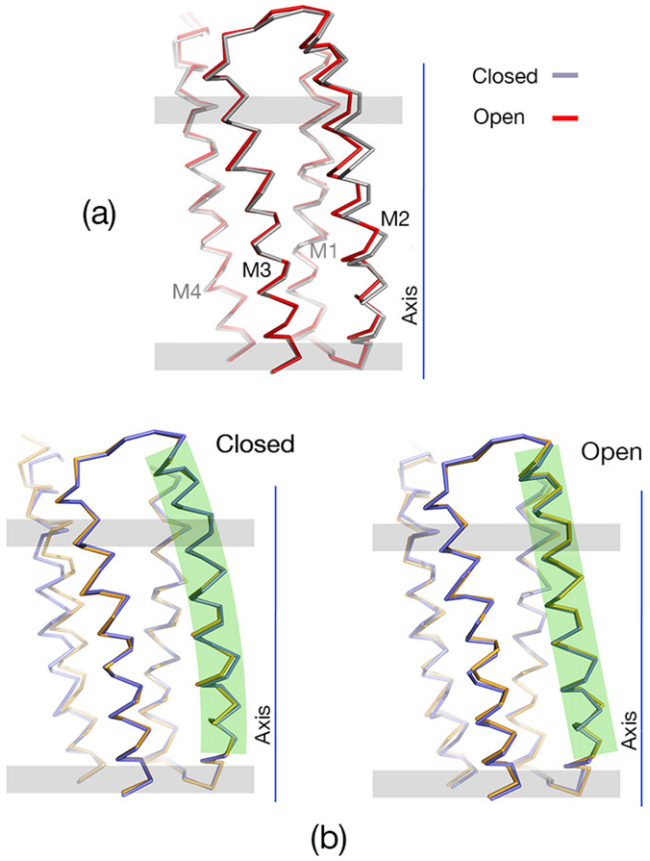

Figure 14. Validation of the small displacements involved in the conformational change to open the acetylcholine receptor channel. (a) Superposition of the membrane helices of the α_γ subunit (see also figure 12(a)) after fitting the atomic model to the closed (grey) and open (red) class density maps. The pore-lining M2 helix straightens when the channel opens, whereas the other helices remain in close-to-fixed positions. (b) Superposition of the helices in pairs (orange and blue traces) after fitting them to independent density maps derived from half-datasets (left: closed class; right: open class). Green shading highlights the alternative bent (closed) and straight (open) conformations of M2. The almost exact superposition of the orange and blue traces demonstrates that the positions and shapes of the well-defined helices M1, M2 and M3 are reproducible, despite the limited resolution of the maps. Reproduced from [54].

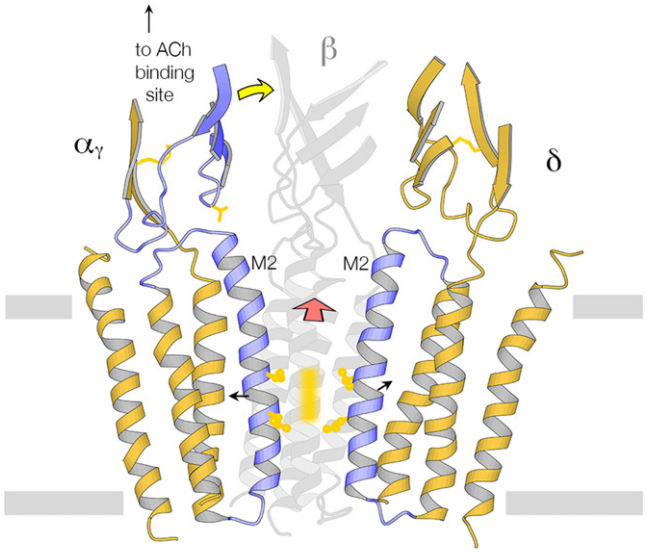

Figure 15. Transduction of a chemical signal to an electrical signal. Acetylcholine on entering the two binding sites induces a concerted conformational change in which the α_γ, β and δ subunits, shown here, play a dominant role. Binding to α_γ triggers a small rearrangement of its outer and inner β-sheets; displacement of the inner sheet of α_γ pushes the adjacent β subunit, causing the membrane helices of β to tilt outward; their tilting action destabilizes the gate and the bent pore-lining M2 helices of α_γ and δ straighten. The altered (open) pore is wider and more polar at the gate, allowing ions to pass through. Arrows denote the movements linking the binding site in α_γ to the gate; yellow arrow: displacement of inner β-sheet of α_γ toward the β subunit; pink arrow: outward displacement and tilting of the β-subunit helices; black arrows: straightening of the pore-lining helices of α_γ and δ in radial and near-tangential directions, opening the gate (yellow bar). The gate is made by a girdle of conserved hydrophobic residues (yellow spheres). The inner β-sheet of α_γ and the pore-lining helices of α_γ and δ, which play key roles in the mechanism, are in blue. Reproduced from [54].

of this structure with that of the closed channel (obtained from the same grids) allowed us to describe the conformational change to open the channel. The indicated displacements, although small, were very precise (figure 14) because the open- and closed-class data sets were both derived by averaging data from many molecules ($\sim 2 \times 10^5$).

We found that all five subunits participate concertedly in communicating the effect of acetylcholine binding to the gate, but that three of them (α_γ, β and δ) play a dominant role. Figure 15 depicts their action. Acetylcholine on coordinating with amino acid residues in the α_γ binding site, induces a small rearrangement of the surrounding outer and inner β-sheets (figure 12(a)), moving the inner sheet in the direction of the β subunit (yellow arrow, figure 15). The β subunit is thereby displaced by about 1 Å, causing its membrane part to tilt outward (pink arrow, figure 15). Tilting of the membrane part of β destabilizes the symmetrical hydrophobic girdle, and the bent pore-lining helices of α_γ and δ are freed to adopt energetically more favoured, straight conformations (black arrows, figure 15). As a result, the hydrophobic constriction forming the gate disappears, and the ions can pass through.

Thus the α_γ subunit, which has a lower affinity for acetylcholine than α_δ, is the main driver of the conformational change, whereas the adjacent β subunit is the main partner communicating it to the membrane. Flexing of oppositely facing pore-lining α-helices is the principal motion determining the closed/open state of the gate. How does this process of chemical-to-electrical transduction, spanning a distance of more than 50 Å, happen in just a few microseconds? I suggest it is through elements integrated into the receptor's architecture that confine the number of essential moving parts and that ensure the required movements are small. In fact, the biggest displacements occur in the two regions most critical for function: at the acetylcholine-binding site (bending inward of loop C) and in the vicinity of the gate (straightening of the pore-lining α-helices). A more detailed

account of this structural transition, discussing the underlying allosteric mechanism and implications for other neurotransmitter-gated ion channels, is given elsewhere [50].

Prospects

In our studies of catalase and purple membrane in 1975, Richard and I recognized the potential of electron microscopy for structure determination of radiation-sensitive unstained specimens. The possibility that the resolution in images could be extended to that attainable by electron diffraction led us to conclude: 'Resolutions close to 3 Å should ultimately be possible' [19]. Now 40 years on, the electron microscope has indeed become an instrument for structure determination at this resolution—and not just from two-dimensional crystals but also from other kinds of ordered specimens (e.g. helical assemblies and icosahedral viruses) and even from individual macromolecules having no symmetry at all (for a recent review, see [56]). No better demonstration of the progress made is a 3.4 Å structure of the relatively small (~300 kDa) TRPV1 ion channel, determined from images of many identical copies oriented randomly in thin films of ice [57].

While clearly the current situation represents a good state of affairs, the pathway leading to it was by no means straightforward, requiring a number of major technological developments. These include higher performance microscopes with field emission guns, giving brighter and more coherent electron illumination; more stable cold stages with improved vacuum environments; and most recently direct electron detectors, which perform better and are both more versatile and adaptable than film [58]. Bigger, faster computers and better algorithms, which apply rigorous statistical methods to analyze the images [59], have also played a crucial part.

Most far-reaching from an experimentalist's perspective, has been the invention of freeze-plunging to retain the sample in amorphous ice [16, 60]. This simple specimen preparation technique is used not only to achieve *in vacuo* preservation of the sample, but also to capture biological molecules in their native membrane or cellular setting, and under ionic conditions close to those that exist *in vivo*. Furthermore, as I have shown, the technique can be adapted to enable analysis of proteins trapped in short-lived conformational states. The risk of misrepresenting true physiological conformations is much diminished by rapid freezing from solution, in comparison with procedures where crystals containing artificial reagents or proteins that have been modified to improve stability, are needed to solve a structure.

This dual capability of providing physiological context and near-atomic resolution is giving electron microscopy some decisive advantages over x-ray crystallography as a means of evaluating complex structures and, in particular, different functional states. These advantages in turn are underpinned by the much wider range of objects to which electron microscopy can be applied, and scope for additional advancement. Already new ways are being devised to reduce radiation-induced motion and associated loss of high resolution information [61]. On-going developments in electron detector technology should soon provide yet further enhancement of signal-to-noise ratio in the recorded images. In the quest to obtain definitive descriptions of biological mechanisms, there is no doubt that the electron imaging approach will become increasingly the one of choice.

Acknowledgments

I was a recipient of the Gregori Aminoff Prize in 1999, along with my colleague, Richard Henderson. I wish to express my deep gratitude to the Royal Swedish Academy of Sciences for this honour. The journey from metals to nerves, as recounted here, surely came about as a result of much good fortune, having truly exceptional scientists as colleagues and through the affectionate and never-ending support of Janet, my wife. My supervisors, Robin Nicholson and Hugh Huxley fostered the beginning stages by giving me the freedom to pursue my own interests, and through example. This work was facilitated by grants from the US National Institutes of Health (GM61941), the Medical Research Council (MRC file reference number U105184294), and by funds from the Louis-Jeantet Foundation.

References

[1] Hirsch P B, Howie A, Nicholson R B, Pashley D W and Whelan M J 1965 *Electron Microscopy of Thin Crystals* (London: Butterworths)
[2] Cundy S L, Metherell A J F, Whelan M J, Unwin P N T and Nicholson R B 1968 Studies of segregation and the initial stages of precipitation at grain boundaries in an alluminium 7 wt% magnesium alloy with an energy analysing electron microscope *Proc. R. Soc.* A **307** 267–81
[3] Unwin P N T, Lorimer G W and Nicholson R B 1969 The origin of the grain boundary precipitate free zone *Acta Metal.* **17** 1363–77
[4] Unwin P N T and Nicholson R B 1969 The nucleation and initial stages of growth of grain boundary precipitates in Al–Zn–Mg and Al–Mg alloys *Acta Metal.* **17** 1379–93
[5] Unwin P N T and Smith G C 1969 The microstructure and mechanical properties of Al-6% Zn-3% Mg *J. Inst. Met.* **97** 299–310
[6] Brandon D G, Ralph B, Ranganathan S and Wald M 1964 A field ion microscope study of atomic configuration at grain boundaries *Acta Met.* **12** 813–21
[7] Ranganathan S 1966 On the geometry of coincidence-site lattices *Acta Cryst.* **21** 197–9
[8] Unwin P N T and Taddei C 1977 Packing of ribosomes in crystals from the lizard, *Lacerta Sicula J. Mol. Biol.* **114** 491–506
[9] Huxley H E 1963 Electron microscope studies on the structure of natural and synthetic protein filaments from striated muscle *J. Mol. Biol.* **7** 281–308
[10] Unwin P N T 1971 Phase contrast and interference microscopy with the electron microscope *Phil. Trans. R. Soc.* B **261** 95–104
[11] Unwin P N T 1972 Electron microscopy of biological specimens by means of an electrostatic phase plate *Proc. R. Soc.* A **329** 327–59

[12] Unwin P N T and Klug A 1974 Electron microscopy of the stacked disk aggregate of tobacco mosaic virus protein I three-dimensional image reconstruction *J. Mol. Biol.* **87** 641–56

[13] Unwin P N T 1974 Electron microscopy of the stacked disk aggregate of tobacco mosaic virus protein II the influence of electron irradiation on the stain distribution *J. Mol. Biol.* **87** 657–70

[14] Finch J T and Klug A 1974 The structural relationship between the stacked disk and helical polymers of tobacco mosaic virus protein *J. Mol. Biol.* **87** 633–40

[15] Taylor K A and Glaeser R M 1974 Electron diffraction of frozen, hydrated protein crystals *Science* **186** 1036–7

[16] Adrian M, Dubochet J, Lepault J and McDowall A W 1984 Cryo-electron microscopy of viruses *Nature* **308** 32–6

[17] Unwin P N T 1975 Beef liver catalase structure: interpretation of electron micrographs *J. Mol. Biol.* **98** 235–42

[18] DeRosier D J and Klug A 1968 Reconstruction of three-dimensional structures from electron micrographs *Nature* **217** 130–4

[19] Unwin P N T and Henderson R 1975 Molecular structure determination by electron microscopy of unstained crystalline specimens *J. Mol. Biol.* **94** 425–40

[20] Henderson R and Unwin P N T 1975 Three-dimensional model of purple membrane obtained by electron microscopy *Nature* **257** 28–32

[21] Taddei C 1972 Ribosome arrangement during oogenesis of *Lacerta sicula* Raf *Exp. Cell Res.* **70** 285–92

[22] Unwin P N T 1977 Three-dimensional model of membrane-bound ribosomes obtained by electron microscopy *Nature* **269** 118–22

[23] Sabatini D D, Tashiro Y and Palade G E 1966 On the attachment of ribosomes to microsomal membranes *J. Mol. Biol.* **19** 503–24

[24] Unwin P N T 1979 Attachment of ribosome crystals to intracellular membranes *J. Mol. Biol.* **132** 69–84

[25] Milligan R A and Unwin P N T 1986 Location of exit channel for nascent protein in 80S ribosome *Nature* **319** 693–5

[26] Kühlbrandt W and Unwin P N T 1982 Distribution of RNA and protein in crystalline eukaryotic ribosomes *J. Mol. Biol.* **156** 431–48

[27] Amunts A, Brown A, Bai X, Llacer J L, Hussain T, Emsley P, Long F, Murshudov G, Scheres S H W and Ramakrishnan V 2014 Structure of the yeast mitochondrial large ribosomal subunit *Science* **343** 1485–9

[28] Unwin P N T and Milligan R A 1982 A large particle associated with the perimeter of the nuclear pore complex *J. Cell Biol.* **93** 63–75

[29] Zampighi G and Unwin P N T 1979 Two forms of isolated gap junctions *J. Mol. Biol.* **135** 451–64

[30] Unwin P N T and Zampighi G 1980 Structure of the junction between communicating cells *Nature* **283** 545–9

[31] Taylor KA and Glaeser RM 1976 Electron microscopy of frozen hydrated specimens *J. Ultrastruct. Res.* **55** 448–56

[32] Taylor K A, Milligan R A, Raeburn C and Unwin P N T 1984 A cold stage for the Philips EM300 electron microscope *Ultramicroscopy* **13** 185–90

[33] Unwin P N T and Ennis P D 1983 Calcium-mediated changes in gap junction structure: evidence from the low-angle x-ray pattern *J. Cell Biol.* **97** 1459–66

[34] Unwin P N T and Ennis P D 1984 Two configurations of a channel-forming membrane protein *Nature* **307** 609–13

[35] Oshima A, Tani K, Hiroaki Y, Fujiyoshi Y and Sosinsky G E 2007 Three-dimensional structure of a human connexin26 gap junction channel reveals a plug in the vestibule *Proc. Natl Acad. Sci. USA* **104** 10034–9

[36] Maeda S, Nakagawa S, Suga M, Yamashita E, Oshima A, Fujiyoshi Y and Tsukihara T 2009 Structure of the connexin 26 gap junction channel at 3.5 Å resolution *Nature* **458** 597–602

[37] Baker T S, Caspar D L D and Murukami W T 1983 Polyoma virus 'hexamer' tubes consist of paired pentamers *Nature* **303** 446–8

[38] Brisson A and Unwin P N T 1984 Tubular crystals of acetylcholine receptor *J. Cell Biol.* **99** 1202–11

[39] Chang H W and Bock E 1977 Molecular forms of acetylcholine receptor. Effects of calcium ions and a sulfhydryl reagent *Biochemistry* **16** 4513–20

[40] Brisson A and Unwin P N T 1985 Quaternary structure of the acetylcholine receptor *Nature* **315** 474–7

[41] Toyoshima C and Unwin N 1988 Ion channel of acetylcholine receptor reconstructed from images of postsynaptic membranes *Nature* **336** 247–50

[42] Toyoshima C and Unwin N 1990 Three-dimensional structure of the acetylcholine receptor by cryo-electron microscopy and helical image reconstruction *J. Cell Biol.* **111** 2623–35

[43] Beroukhim R and Unwin N 1997 Distortion correction of tubular crystals: improvements in the acetylcholine structure *Ultramicroscopy* **70** 57–81

[44] Fujiyoshi Y, Mizuasaki T, Morikawa K, Yamagishi H, Aoki Y, Kihara H and Harada Y 1991 Development of a superfluid helium stage for high resolution electron microscopy *Ultramicroscopy* **38** 241–51

[45] Miyazawa A, Fujiyoshi Y, Stowell M and Unwin N 1999 Nicotinic acetylcholine receptor at 4.6 Å resolution: tranverse tunnels in the channel wall *J. Mol. Biol.* **288** 765–86

[46] Miyazawa A, Fujiyoshi Y and Unwin N 2003 Structure and gating mechanism of the acetylcholine receptor pore *Nature* **423** 949–55

[47] Unwin N 2005 Refined structure of the nicotinic acetylcholine receptor at 4 Å resolution *J. Mol. Biol.* **346** 967–89

[48] Beckstein O and Sansom M S 2004 The influence of geometry, surface character and flexibility on the permeation of ions and water through biological pores *Phys. Biol.* **1** 42–52

[49] Colquhoun D and Ogden D C 1988 Activation of ion channels in the frog endplate by high concentrations of acetylcholine *J. Physiol.* **395** 131–59

[50] Unwin N 2013 Nicotinic acetylcholine receptor and the structural basis of neuromuscular transmission: insights from *Torpedo* postsynaptic membranes *Q. Rev. Biophys.* **46** 283–322

[51] DaCosta C J and Baenziger J E 2009 A lipid-dependent uncoupled conformation of the acetylcholine receptor *J. Biol. Chem.* **284** 17819–25

[52] DaCosta C J, Medaglia S A, Lavigne N, Wang S, Carswell C L and Baenziger J E 2009 Anionic lipids allosterically modulate multiple nicotinic acetylcholine receptor conformational equilibria *J. Biol. Chem.* **284** 33841–9

[53] Berriman J and Unwin N 1994 Analysis of transient structures by cryo-microscopy combined with rapid mixing of spray droplets *Ultramicroscopy* **56** 241–52

[54] Unwin N and Fujiyoshi Y 2012 Gating movement of acetylcholine receptor caught by plunge-freezing *J. Mol. Biol.* **422** 617–34

[55] Kuffler S W and Yoshikami D 1975 The number of transmitter molecules in a quantum: an estimate from iontophoretic application of acetylcholine at the neuromuscular junction *J. Physiol.* **251** 465–82

[56] Crowther R A 2010 From envelopes to atoms: the remarkable progress of biological electron microscopy *Adv. Prot. Chem. Struct. Biol.* **81** 1–32

[57] Liao M, Cao E, Julius D and Cheng Y 2013 Structure of the TRPV1 ion channel determined by electron cryo-microscopy *Nature* **504** 107–12

[58] Kühlbrandt W 2014 Cryo-EM enters a new era *Elife* **3** e03678

[59] Scheres S H W 2012 RELION: implementation of a Bayesian approach to cryo-EM structure determination *J. Struct. Biol.* **180** 519–30

[60] Dubochet J, Adrian M, Chang JJ, Homo JC, Lepault J, McDowall JW and Schultz P 1988 Cryo-electron microscopy of vitrified specimens *Q. Rev. Biophys.* **21** 129–228

[61] Russo C J and Passmore L A 2014 Controlling protein adsorption on graphene for cryo-EM using low energy hydrogen plasmas *Nat. Methods* **11** 649–52